Magnetic compensation, field-dependent magnetization reversal, and complex magnetic ordering in Co_2TiO_4

S. Nayak,[1] S. Thota,[1,*] D. C. Joshi,[1] M. Krautz,[2] A. Waske,[2] A. Behler,[2] J. Eckert,[3,4] T. Sarkar,[5] M. S. Andersson,[5] R. Mathieu,[5] V. Narang,[6] and M. S. Seehra[6,†]

[1]*Department of Physics, Indian Institute of Technology Guwahati, Guwahati-781039, Assam, India*

[2]*IFW Dresden, Institute for Complex Materials, P.O. Box 270116, D-01171 Dresden, Germany*

[3]*Erich Schmid Institute of Materials Science, Austrian Academy of Sciences, Jahnstraße 12, A-8700 Leoben, Austria*

[4]*Department Materials Physics, Montanuniversität Leoben, Jahnstraße 12, A-8700 Leoben, Austria*

[5]*Department of Engineering Sciences, Uppsala University, Box 534, SE-751 21 Uppsala, Sweden*

[6]*Department of Physics and Astronomy, West Virginia University, Morgantown, West Virginia 26506, USA*

(Received 25 October 2015; published 23 December 2015)

The complex nature of magnetic ordering in the spinel Co_2TiO_4 is investigated by analyzing the temperature and magnetic field dependence of its magnetization (M), specific heat (C_p), and ac magnetic susceptibilities χ' and χ''. X-ray diffraction of the sample synthesized by the solid-state reaction route confirmed the spinel structure whereas x-ray photoelectron spectroscopy shows its electronic structure to be $Co_2TiO_4 = [Co^{2+}][Co^{3+}Ti^{3+}]O_4$. From analysis of the temperature dependence of the dc paramagnetic susceptibility, the magnetic moments $\mu(A) = 3.87\,\mu_B$ and $\mu(B) = 5.19\,\mu_B$ on the A and B sites are determined with $\mu(B)$ in turn yielding $\mu(Ti^{3+}) = 1.73\,\mu_B$ and $\mu(Co^{3+}) = 4.89\,\mu_B$. Analysis of the dc and ac susceptibilities combined with the weak anomalies observed in the C_p vs T data shows the existence of a quasi-long-range ferrimagnetic state below $T_N \sim 47.8\,K$ and a compensation temperature $T_{comp} \sim 32\,K$, the latter characterized by sign reversal of magnetization with its magnitude depending on the applied magnetic field and the cooling protocol. Analysis of the temperature dependence of M (field cooled) and M (zero field cooled) data and the hysteresis loop parameters is interpreted in terms of large spin clusters. These results in Co_2TiO_4, significantly different from those reported recently in isostructural $Co_2SnO_4 = [Co^{2+}][Co^{2+}Sn^{4+}]O_4$, warrant further investigations of its magnetic structure using neutron diffraction.

I. INTRODUCTION

Magnetic spinels are a remarkable class of materials, not only for their many applications, but also because of a wealth of new physics that continues to emerge from their fundamental investigations [1–6]. These properties result from many variations of the magnetic and nonmagnetic ions that can be accommodated on the tetrahedral A sites and the octahedral B sites in the AB_2O_4 spinel structure, thus affecting the magnitudes of the superexchange interactions J_{AA}, J_{BB}, and J_{AB} [7–9]. The presence of nonmagnetic ions on either the A or the B sites can lead to magnetic frustration [10–12]. For example, for normal spinels like $ZnFe_2O_4 = [Zn^{2+}][Fe_2^{3+}]O_4^4$ and $MgMnO_3 = (3/4)\{Mg^{2+}\}[[Mg^{2+}_{1/3}Mn^{4+}_{4/3}\square_{1/3}]O_4]$ [13], which have magnetic ions only on the B sites with '$\square$' as vacancy, the magnetic ground state is highly frustrated, as first predicted by Anderson in such a case [14].

We have recently reported on the nature of magnetic ordering in the spinel Co_2SnO_4 [15,16], for which the distributions of the ions on the A and the B sites was established to be $[Co^{2+}]_A[Co^{2+}Sn^{4+}]_BO_4$ by x-ray photoelectron spectroscopy (XPS). Analysis of the temperature dependence of both the ac and dc magnetic susceptibilities and specific heat measurements showed that Co_2SnO_4 is a ferrimagnet due to

slightly different magnetic moments of Co^{2+} on the A and the B sites below 41 K, with some dynamical properties [15,16].

Co_2TiO_4 is isostructural to Co_2SnO_4 in which Sn is replaced by Ti in the former. Although a number of papers have previously reported on the nature of magnetism in Co_2TiO_4, the results have been controversial. The magnetic studies of Hubsch and Gavoille [17] and Gavoille *et al.* [18] reported ferrimagnetic ordering at $T_N \sim 55\,K$ followed by spin-glass transition at $T_{SG} \sim 46\,K$. However, later ac susceptibility studies by Srivastava *et al.* [19], showed no indication of $T_N \sim 55\,K$, rather only a single peak in χ_{ac} near 48 K when $H_{dc} = 0$. In the studies of the temperature dependence of specific heat C_p of Co_2TiO_4 by Ogawa and Waki [20], only a weak peak in C_p vs T was reported near 49 K, which was associated with magnetic ordering, again signaling the absence of a transition near 55 K. The magnetic studies by Hubsch and Gavoille also showed a magnetic compensation point near 30 K [17]. In all these reported studies, it has been assumed that the electronic state of Ti in Co_2TiO_4 is Ti^{4+}, similar to Sn^{4+} in Co_2SnO_4.

In this paper, we revisit the nature of magnetic ordering in Co_2TiO_4 in order to address the unsettled issues listed above and to examine the similarities and differences in the magnetic properties of Co_2TiO_4 and Co_2SnO_4. For example, why the compensation point observed in Co_2TiO_4 near 30 K [17] is not observed in Co_2SnO_4 [16] if the electronic states of Co in the two systems are similar. In our investigations of Co_2TiO_4, we have employed x-ray diffraction (XRD), XPS, temperature and magnetic field dependence of the ac and

*subhasht@iitg.ac.in

†mseehra@wvu.edu

dc magnetic susceptibilities, and temperature and magnetic field dependence of specific heat measurements to unravel the nature of magnetic ordering in this system. From these studies, it is shown that the electronic state of Ti in Co_2TiO_4 is not Ti^{4+} but primarily Ti^{3+}, resulting in the configuration $[Co^{2+}][Co^{3+}Ti^{3+}]O_4$. In contrast to the case of Co_2SnO_4, this gives very different magnetic moments on the *A* and the *B* sites in Co_2TiO_4, which are also confirmed from the analysis of the temperature dependence of the paramagnetic susceptibility. It is argued that these distinctly different magnetic moments on the *A* and the *B* sites lead to the observed magnetic compensation near 30 K. Also, our studies rule out any magnetic transition near 55 K; instead, a transition to a quasi-long-range ferrimagnetic state akin to that of Co_2SnO_4 [15,16] is found below 48 K. Some new results in Co_2SnO_4 are also presented for comparison with Co_2TiO_4. Details of these results determined from multitechnique investigations and their discussion and analysis are presented below.

II. EXPERIMENTAL PROCEDURES

The bulk grain size polycrystalline Co_2TiO_4 and Co_2SnO_4 samples were synthesized by the standard solid-state reaction method starting with stoichiometric amounts of Co_3O_4, TiO_2, and SnO_2 as precursors. Appropriate amounts of these materials were first ground in an agate mortar and sieved through a 240 mesh. The mixed powders were pressed into pellets of diameter $\sim$13 mm using a hydraulic press with a maximum load of 5 ton/cm^2. The pellets of Co_2TiO_4 were finally sintered at 1120 °C (1350 °C for Co_2SnO_4 [16]) for 18 h in air to yield the desired compound without any impurities or unreacted precursors. The structural characterization was performed using a Rigaku x-ray diffractometer (model TTRAX III) with Cu Kα radiation ($\lambda = 1.54056$ Å) followed by Rietveld refinement of the diffraction patterns using the FullProf program, which confirmed the phase purity of the samples (Fig. 1). Both dc magnetization and frequency dependence (0.17–1.2 kHz) of ac magnetic susceptibility measurements were performed using a superconducting quantum interference device (SQUID) based magnetometer from Quantum Design with temperature capabilities of 2–320 K and magnetic field (H) up to $\pm$90 kOe. The low-temperature heat capacity data [$C_p(T)$] was recorded by means of a physical property measurement system (PPMS) from Quantum Design. The surface chemical composition of both the bulk samples were analyzed by means of XPS measurements performed with a dual source VG Microtech XPS microprobe system using Al Kα radiation (1486.8 eV) source at a base pressure of 8×10^{-10} Torr. The XPS data were collected from 0 to 1100 eV of binding energy (B.E.) which is acquired with constant pass energy of 100 eV. All the spectra were analyzed using Gaussian-Lorentzian curve fitting.

III. STRUCTURAL AND ELECTRONIC CHARACTERIZATION

A. X-ray diffraction

Figure 1 shows the XRD pattern of the polycrystalline samples of both Co_2TiO_4 and Co_2SnO_4 along with their Rietveld refinement done using the FullProf program. These
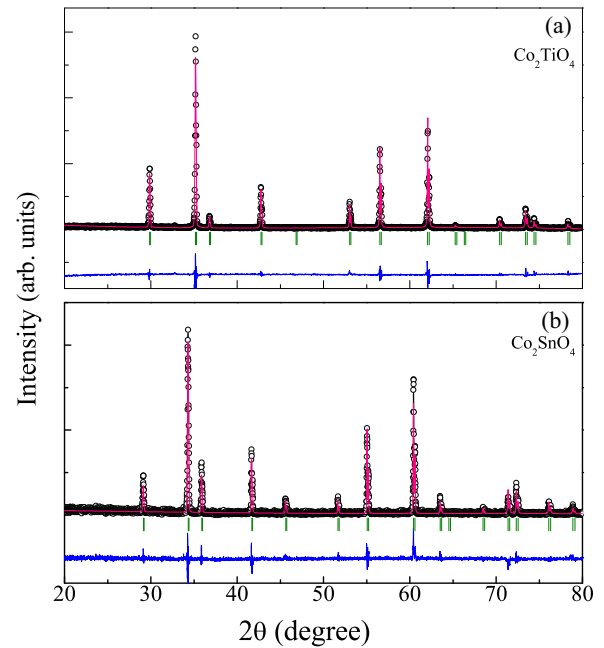

FIG. 1. (Color online) XRD patterns together with the Rietveld refined data of (a) Co_2TiO_4 and (b) Co_2SnO_4. The blue lines at the bottom represent difference between the measured and simulated patterns.

patterns are consistent with the standard cubic spinel phase with space group $Fd-3m$ (227). However, the lattice parameter obtained for Co_2TiO_4 ($a = 8.45$ Å) is slightly less than that of Co_2SnO_4 ($a = 8.66$ Å). Such variation in the lattice parameters is generally associated with the different ionic radii of the constituent elements. Since the ionic radius of tetravalent stannous ion ($Sn^{4+} = 0.69$ Å) is slightly greater than that of the titanium ion (either $Ti^{4+} = 0.605$ Å or $Ti^{3+} = 0.67$ Å), larger unit cell dimensions of Co_2SnO_4 as compared to that of Co_2TiO_4 are expected. On the other hand, the ionic radius of Co^{2+} ions in tetrahedral sites with coordination number four is smaller ($Co^{2+}_{Tetra-A} = 0.58$ Å) than that in high spin octahedral sites with coordination number six ($Co^{2+}_{Octa-B} = 0.745$ Å). Table I summarizes the bond lengths and bond angles in both Co_2TiO_4 and Co_2SnO_4 estimated from the refinement process. It is evident that the average bond length (*B*-O) between the oxygen ion and elements present in the octahedral sites of Co_2SnO_4 is higher than that in Co_2TiO_4, while the reverse is true for the tetrahedral sites. Such differences in bond lengths at the octahedral and tetrahedral sites in the two systems result from the difference in the ionic sizes. Since the Sn ion is larger than the Ti ions, the *B*-O bond length in Co_2SnO_4 is greater than that in Co_2TiO_4, resulting in a larger lattice parameter of Co_2SnO_4 than that of Co_2TiO_4 as observed experimentally.

B. X-ray photoelectron spectroscopy

For a detailed understanding of the electronic state of elements present in both systems, XPS measurements with Al-Kα x-rays as source were performed. Figure 2 shows the intensity of XPS spectra vs binding energy of the Co–$2p$ core levels for pure Co_3O_4, Co_2TiO_4, and Co_2SnO_4 systems. All these spectra exhibit two sharp peaks characteristic of

TABLE I. The list of lattice parameters ($a = b = c$), bond lengths, and bond angles in Co_2SnO_4 and Co_2TiO_4. (The interaxial angles $\alpha = \beta = \gamma = 90°$)

System	Lattice parameter	Bond length		Bond angle	
		A-O	B-O	A-O-B	B-O-B
Co_2TiO_4	8.45 ± 0.01 Å	1.98 ± 0.011 Å	2.03 ± 0.017 Å	$121.68° \pm 0.612°$	$94.95° \pm 0.478°$
Co_2SnO_4	8.66 ± 0.02 Å	1.88 ± 0.02 Å	2.16 ± 0.021 Å	$125.01° \pm 0.625°$	$90.37° \pm 0.452°$

Co–$2p_{3/2}$ and Co–$2p_{1/2}$ together with the weak intensity satellite peaks shown by arrows at 786.7 eV (S_1) and 802.91 eV (S_2). It is well known that both Co^{2+} and Co^{3+} exhibit similar binding energy peaks in XPS data with a sharp transition near 780 eV identified with $2p_{3/2}$ level and a second peak near 796 eV identified with $2p_{1/2}$ level. However, the energy splitting (ΔE) between the two levels due to spin-orbit coupling should be different for the Co^{2+} and Co^{3+} configurations with $\Delta E = 15.0$ eV for Co^{3+} and $\Delta E = 15.7$ eV for Co^{2+} [21–23]. The XPS data in Fig. 2(a) for the spinel Co_3O_4, which contains both Co^{2+} and Co^{3+} ions distributed on the A and the B sites as $[Co^{2+}]_A[2Co^{3+}]_BO_4$, clearly show the presence of doublet at $D_1 = 779.84$ eV and $D_2 = 780.34$ eV for the Co–$2p_{3/2}$ level and a doublet for the Co–$2p_{1/2}$ level centered at $D_3 = 794.84$ eV and $D_4 = 796.09$ eV. The separations between the doublet peaks are $\Delta E_{D_1-D_3} = 15$ eV and $\Delta E_{D_2-D_4} = 15.75$ eV, which are close to the above-mentioned values for Co^{3+} and Co^{2+}, respectively, thus confirming the

FIG. 2. (Color online) The XPS of Co−$2p$ peaks of (a) Co_3O_4, (b) Co_2TiO_4, and (c) Co_2SnO_4.

presence of Co^{3+} and Co^{2+} in Co_3O_4. These results are in good agreement with the previously reported data by Chuang *et al.* [24].

Figure 2(b) shows the core level XPS spectra of Co–$2p_{3/2}$ and Co–$2p_{1/2}$ for the spinel Co_2TiO_4. If the distribution of ions in Co_2TiO_4 is $[Co^{2+}][Co^{2+}Ti^{4+}]O_4$, as has been assumed in previous studies, then this system should not exhibit any Co^{3+} character. However, our XPS studies in Co_2TiO_4 [Fig. 2(b)] show clear signatures of Co^{3+} state in addition to the Co^{2+} state in terms of doublets discussed above for Co_3O_4. For the XPS spectra of Co–$2p_{3/2}$ and Co–$2p_{1/2}$ levels, the simulated Gaussian-Lorentzian fitting yields two different intensity peaks with narrow separation labeled by P_1 and P_2 for $2p_{3/2}$, and P_3 and P_4 for $2p_{1/2}$, as shown in Fig. 2(b). The observed difference between the doublets $\Delta E_{P_1-P_3} = 14.98$ eV and $\Delta E_{P_2-P_4} = 15.43$ eV provides the signatures of the Co^{3+} and Co^{2+}, respectively, as compared to the expected values of $\Delta E = 15.0$ eV for Co^{3+} and $\Delta E = 15.7$ eV for Co^{2+} [16]. On the other hand, for the Co_2SnO_4 case, the data shown in Fig. 2(c) give, $\Delta E = 15.7$ eV characteristic of Co^{2+} only, and no additional signatures for the Co^{3+} state are noticed in Co_2SnO_4, as also reported in our recent study [16].

Next, we consider the electronic states of Ti, Sn, and O. For TiO_2 with Ti^{4+} as the electronic state of titanium, the binding energy for the Ti–$2p_{3/2}$ state is observed at 459.5 eV [25]. However, in the case of Co_2TiO_4, the maximum intensity peak for Ti–$2p_{3/2}$ appears at 457.65 eV [Fig. 3(a)], while the second maximum intensity peak corresponding to Ti–$2p_{1/2}$ is centered at 463.53 eV. This result rules out the presence of Ti^{4+} state in Co_2TiO_4. Instead, the observed position of the peak at 457.65 eV agrees with the previously reported data of Ti^{3+} surface defects at 457.7 eV in the TiO_2 system [26]. In addition, these results also rule out the presence of any metallic Ti ions in the Co_2TiO_4 matrix, which usually show their signatures in XPS spectra at 454 eV. For Co_2SnO_4, the sharp peaks observed at 485.65 and 494.8 eV and a weak shoulder at 496.75 eV in Fig. 3(b) are the characteristic signatures of Sn^{4+} state [21,27]. Finally, Fig. 3(c) shows O–$1s$ core level spectra for all the three systems with some signature of weakly bound surface oxygen at a binding energy close to 533 eV [21–25,28,29]. The major conclusions from these comparative XPS studies in Co_3O_4, Co_2TiO_4, and Co_2SnO_4 are that, electronically, $Co_2TiO_4 = [Co^{2+}][Co^{3+}Ti^{3+}]O_4$, whereas $Co_2SnO_4 = [Co^{2+}][Co^{2+}Sn^{4+}]O_4$. This difference in the electronic state of Co ions on the B sites of these two systems has never been reported before to our knowledge, and as we will show, it leads to major differences in the observed magnetic properties of Co_2TiO_4 from those of Co_2SnO_4. Below, we present detailed magnetic studies of Co_2TiO_4
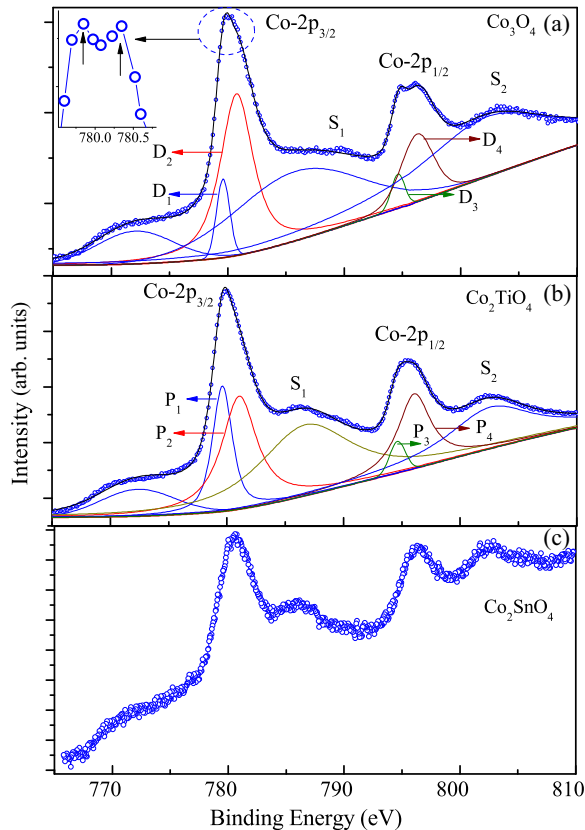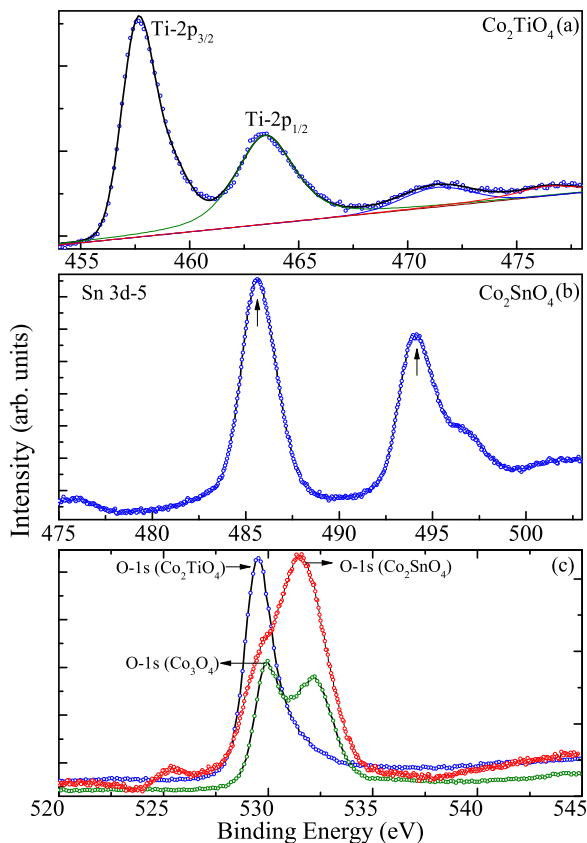
FIG. 3. (Color online) The XPS of (a) Ti−2p, (b) Sn−3d, (c) O−1s peaks of Co_2TiO_4, Co_2SnO_4, and Co_3O_4 systems.

FIG. 4. (Color online) Temperature variation of the inverse paramagnetic susceptibility $\chi^{-1}(T)$ of Co_2TiO_4 and Co_2SnO_4 systems. The solid lines are best fits to the Néel's expression for ferrimagnets discussed in the text.

along with their discussion and interpretation, accompanied by comparison with Co_2SnO_4 where appropriate.

IV. RESULTS FROM MAGNETIC MEASUREMENTS

A. Temperature dependence of the paramagnetic susceptibility

The temperature dependence of dc magnetic susceptibility (χ) of both Co_2TiO_4 and Co_2SnO_4 for $T > 45$ K recorded under zero field cooled (ZFC) conditions is shown in Fig. 4; here, χ^{-1} vs T plots are shown with blue circles and green squares as experimental points and red and brown solid lines as fits to the Néel expression for ferrimagnets viz. $(1/\chi) = (T/C) + (1/\chi_0) - [\sigma_0/(T - \theta)]$. The fit for Co_2TiO_4 yields the following parameters: $\chi_0 = 41.92 \times 10^{-3}$ emu/mol-Oe, $\sigma_0 = 31.55$ mol-Oe-K/emu, $C = 5.245$ emu K/mol Oe, $\theta = 49.85$ K. The ratio $C/\chi_0 = T_a = 125.1$ K represents the strength of the antiferromagnetic exchange coupling between the spins on the A and B sites and is often termed as the asymptotic Curie temperature T_a. In Table II, various fitting parameters obtained from the Néel expression for ferrimagnetism of both Co_2TiO_4 and Co_2SnO_4 are summarized. The effective magnetic moment $\mu_{eff} = 6.5 \mu_B$ per formula unit (f.u.) of Co_2TiO_4 is determined using $C = N \mu_{eff}^2/3 k_B$. A similar calculation yielded $\mu_{eff} = 6.25 \mu_B$ per f.u. of $Co_2SnO_4 = [Co^{2+}][Co^{2+}Sn^{4+}]O_4$. Using $\mu^2 = [\mu(A)]^2 + [\mu(B)]^2$ with $\mu(A) = 3.87 \mu_B$ for Co^{2+} ions on the A sites with spin $S = 3/2$ and $g = 2$ since its tetrahedral coordination does not allow orbital contribution, yields $\mu(B) = 4.91 \mu_B$ for Co_2SnO_4. This
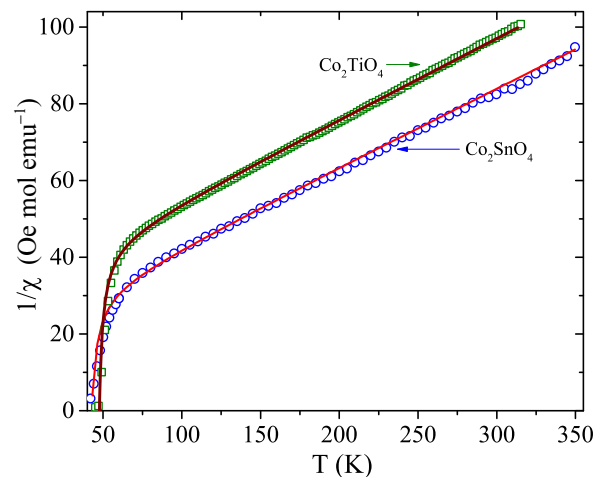
argument for Co_2SnO_4 yields ferrimagnetism below T_N with net small moment of $1.04 \mu_B$ per f.u.

For Co_2TiO_4, with the electronic configuration of $[Co^{2+}][Co^{3+}Ti^{3+}]O_4$ determined using XPS, the above analysis yields $\mu_{eff} = 6.5 \mu_B$ per f.u. Again, using $\mu(A) = 3.87 \mu_B$ for Co^{2+} ions on the A site as in Co_2SnO_4 yields $\mu(B) = 5.19 \mu_B$ for ions on the B site. The trivalent titanium ion Ti^{3+} with its $3d^1$ electronic configuration has magnetic moment $\mu = 1.73 \mu_B$ yielding $\mu(Co^{3+}) = 4.89 \mu_B$ as the moment for the Co^{3+} ion on the B site. In the high spin state, Co^{3+} ions should have spin only $\mu = 4.9 \mu_B$, which agrees with the above estimate. So an important conclusion from this comparative analysis of the paramagnetic susceptibilities is that $\mu_{eff} = 6.5 \mu_B$ per f.u. of Co_2TiO_4 is higher than that in Co_2SnO_4. This leads to the calculated net ferrimagnetic moment of $\mu = 1.32 \mu_B$ per f.u. below T_N, which is higher than $\mu = 1.04 \mu_B$ per f.u. of Co_2SnO_4 below its T_N. This information is used below to explain the observed differences in the measured magnetic properties of Co_2TiO_4 against Co_2SnO_4 below T_N. Another important difference between the two systems is that, in Co_2TiO_4, the B site is occupied by Co^{3+} and Ti^{3+}, both of which have magnetic moments unlike the case of Co_2SnO_4 in which the Sn^{4+} ion on the B site does not have a magnetic moment. Therefore, the effects of magnetic dilution should be less prominent in Co_2TiO_4.

B. Temperature dependence of the dc magnetic susceptibilities

The temperature dependence of the dc magnetic susceptibilities $\chi_{dc} = M/H_{dc}$ determined from the measured magnetization (M) in the presence of external magnetic field $H_{dc} = 50, 100, 500, 1000,$ and $10,000$ Oe is shown in Fig. 5 for Co_2TiO_4. The data are shown for both the traditional ZFC and field cooled (FC) cases. The significant features of the data are χ peaking at a temperature near 46 K, suggesting ferrimagnetic ordering, and a crossover in sign for χ (ZFC) and χ (FC) at a compensation temperature near 32 K, where the magnetization of the two sublattices balance each other.

TABLE II. The list of various parameters obtained from the Néel fits of χ^{-1} vs T curve recorded under zero-field-cooled condition.

System	C(emu K mol^{-1}Oe^{-1})	χ_o(emu mol^{-1}Oe^{-1})	σ_o(emu^{-1}Oe mol K)	θ (K)	$\mu_{\mathrm{eff}}(\mu_B)$	$\mu(A)$ (μ_B)	$\mu(B)$ (μ_B)
Co$_2$TiO$_4$	5.245	0.0419	31.55	49.85	6.5	3.87	5.19
		N_{AA}	N_{AB}	N_{BB}	J_{AA}	J_{AB}	J_{BB}
		17.319	35.700	12.720	3.25 k_B	4.47 k_B	3.18 k_B
Co$_2$SnO$_4$	4.889	0.0436	102.370	39.5	6.25	3.87	4.91
		N_{AA}	N_{AB}	N_{BB}	J_{AA}	J_{AB}	J_{BB}
		21.564	33.201	10.678	4.05 k_B	5.26 k_B	4.28 k_B

These observations are similar to those reported by Hubsch and Gavoille [17] in Co$_2$TiO$_4$ and are discussed in more detail later. The temperature dependence of the magnetization (M) for the ZFC and FC cases under applied H_{dc} = 5, 10, 20, 30, and 40 kOe is shown in Fig. 6. Several features of the data are noteworthy: (i) the compensation temperature $T_{\mathrm{comp}} \simeq 32$ K is independent of applied H_{dc}, and compensation is not complete in that M at T_{comp} is not zero but increases with increase in H_{dc}; (ii) the position of the peak temperature near 46 K shifts slightly to higher temperatures with increase in H_{dc}; and (iii) the temperature for which M (FC) bifurcates from M (ZFC) shifts to lower temperature with increase in H_{dc}. Very similar features have been observed in other spinel compounds as well, for example, in the Ni-Fe-Sb-O spinel [30].

In order to compare the above observations in Co$_2$TiO$_4$ with similar measurements in Co$_2$SnO$_4$, new data on Co$_2$SnO$_4$ [15,16] are shown in Fig. 7 for the ZFC and FC cases in H = 100, 500, 1000, and 5000 Oe. Although there are some similarities with the data for Co$_2$TiO$_4$ in Fig. 5, the behavior near the compensation temperature of 32 K in Co$_2$TiO$_4$ is not observed in Co$_2$SnO$_4$. Instead, there is a bifurcation of the FC and ZFC data beginning near 7 K, which is field independent, and a second bifurcation at higher temperatures, the location of which is field dependent. More information on these differences between the two systems become evident from the behavior of the hysteresis loop parameters discussed later.
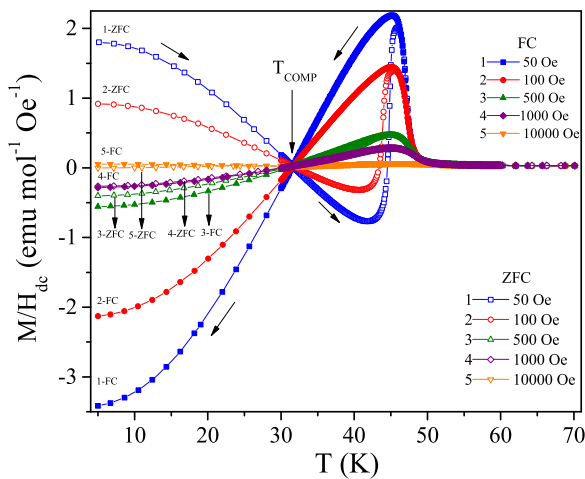
C. Temperature dependence of the ac magnetic susceptibility

The temperature dependence of the ac magnetic susceptibilities χ' and χ'' were measured using a frequency of 2 Hz with $h_{\mathrm{ac}} = 4$ Oe superimposed with various dc fields H_{dc} between 0, 10, 20, and 30 Oe. The results of the plots of χ' and χ'' vs temperature in Fig. 8 show splitting of a single peak near 46.5 K into two peaks when H_{dc} is increased. In the χ' vs T data, the higher temperature peak shifts to the higher temperature side with increase in H_{dc}, whereas the reverse is true for the lower temperature peak. The transition at 46.5 K was probed further by measuring temperature dependence of χ' and χ'' at nine different frequencies f_m between 0.17 and 1202 Hz using $h_{\mathrm{ac}} = 4$ Oe and $H_{\mathrm{dc}} = 0$. The results are plotted in Fig. 9. For χ', the peak at 46.8 K measured at the lowest frequency of 0.17 Hz shifts to higher temperatures with increase in frequency, approaching near 47.11 K at $f_m = 1202$ Hz.

This kind of frequency dependence of the peak in the ac susceptibility curves seems to be qualitatively quite similar to what we had observed earlier in Co$_2$SnO$_4$ [16]. However, a detailed quantitative analysis of the data revealed a marked difference between the two systems. As in the case of Co$_2$SnO$_4$ [16], we tried to analyze the frequency dependence seen in Co$_2$TiO$_4$ using two scaling laws: (i) the Vogel-Fulcher law, which is given by the expression $\tau = \tau_0 \exp[\frac{E_a}{k_B(T-T_0)}]$, where τ_0 is the relaxation time constant, T_0 is a measure of the interaction between magnetic clusters, k_B is the Boltzmann constant, and E_a is an activation energy parameter; and (ii) the power
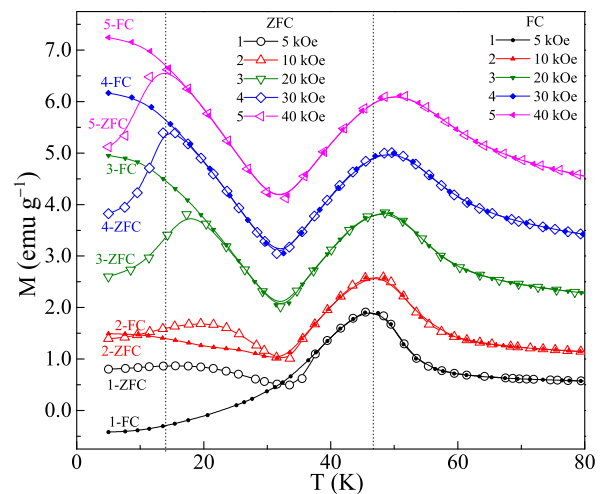

FIG. 5. (Color online) Temperature dependence of dc magnetic susceptibility $\chi(T)[= M/H_{\mathrm{dc}}(T)]$ for Co$_2$TiO$_4$ measured under both ZFC and FC conditions recorded at various magnetic fields in the range 50 Oe $\leqslant H_{\mathrm{dc}} \leqslant$ 10 kOe.

FIG. 6. (Color online) High-field (5 kOe $\leqslant H_{\mathrm{dc}} \leqslant$ 40 kOe) magnetization (M) vs temperature (T) data for Co$_2$TiO$_4$ measured under both the ZFC and FC conditions.

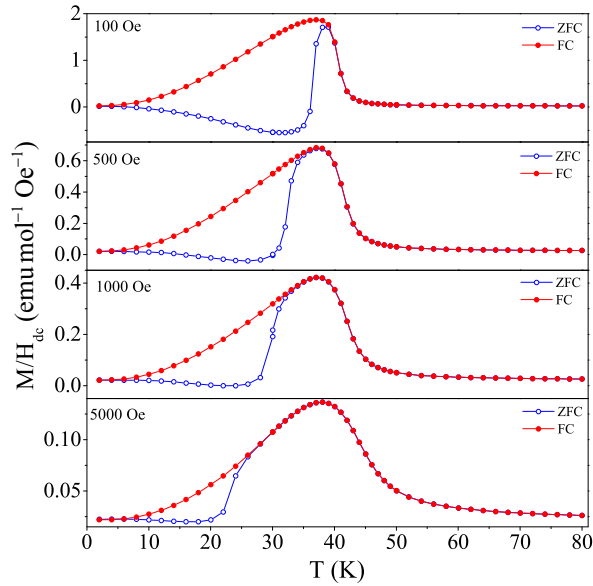FIG. 7. (Color online) Temperature dependence of dc magnetic susceptibility $\chi(T)[= M/H_{dc}(T)]$ for Co_2SnO_4 measured under both ZFC and FC conditions recorded at various magnetic fields.

FIG. 9. (Color online) Temperature dependence of ac magnetic susceptibilities (a) $\chi'(T)$ and (b) $\chi''(T)$ of Co_2TiO_4 measured at various frequencies between 0.17 and 1202 Hz under warming conditions using $h_{ac} = 4$ Oe and $H_{dc} = 0$ Oe.

law, which describes the critical slowing down in a spin-glass phase transition at T_g, and is given by $\tau = \tau_0[(\frac{T}{T_g}) - 1]^{-z\nu}$, where T_g is the freezing temperature, τ_0 is related to the relaxation of the individual cluster magnetic moment, and $z\nu$ is a critical exponent. Here, $\tau = \frac{1}{\omega} = \frac{1}{2\pi f}$. While for Co_2SnO_4 [16], we could obtain physically reasonable fit parameters using both the Vogel-Fulcher law as well as the power law albeit using a very limited temperature range, for Co_2TiO_4, the situation is different. In Fig. 10, we show the best representation of the data that was obtained using the Vogel-Fulcher law, with $T_0 = 45.8$ K and $\tau_0 = 3.2 \times 10^{-16}$ s.
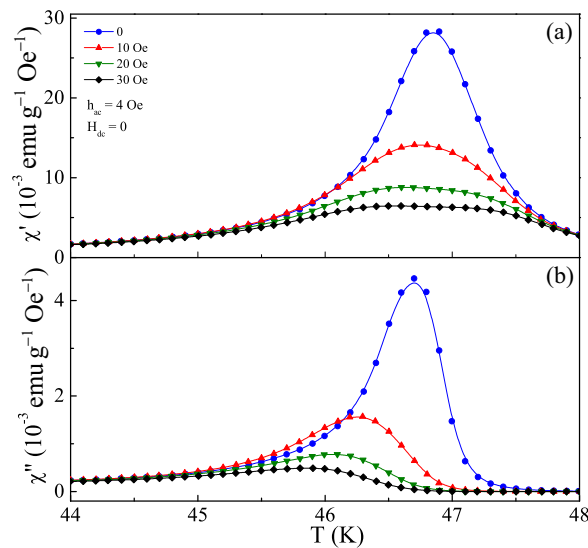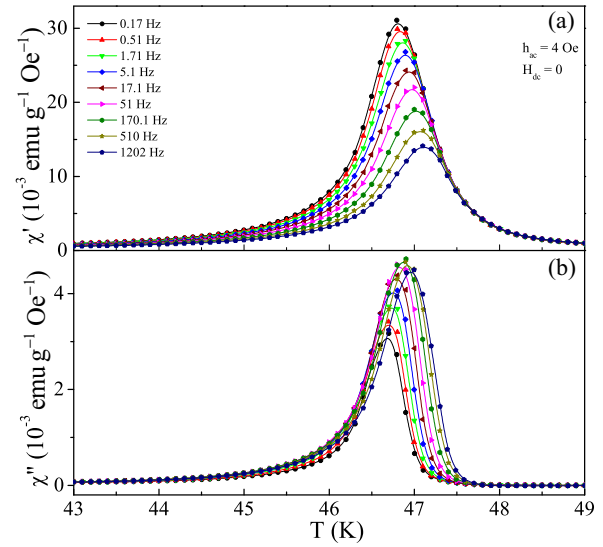
However, an attempt to fit the data using the power law, yielded quite unphysical values of the fit parameters (viz. $\tau_0 \sim 10^{-33}$ s and $z\nu > 16$), indicating the lack of SG phase transition.

D. Temperature dependence of the hysteresis loop parameters

Hysteresis loop measurements of M vs H for the Co_2TiO_4 sample were performed at selected temperatures between 5 and 60 K in the magnetic field range of -90 to $+90$ kOe. The measurements were done in the ZFC (FC) protocol in which the sample is cooled in $H_{dc} = 0$ Oe ($H_{dc} = 20$ kOe) from the paramagnetic state to the measuring temperature followed by measurements of M vs H. For the data at the next temperature, the sample was again warmed to the paramagnetic state and cooled back similarly to the next measurement temperature. Hysteresis loops at four selected
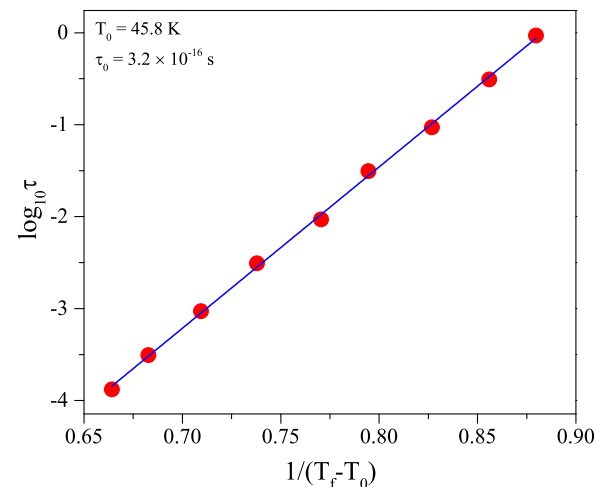

FIG. 8. (Color online) (a) Temperature variation of the ac magnetic susceptibility (a) $\chi'(T)$, and (b) $\chi''(T)$ for Co_2TiO_4 measured at 2 Hz in $h_{ac} = 4$ Oe with superposed dc bias fields $H_{dc} = 0, 10, 20,$ and 30 Oe.

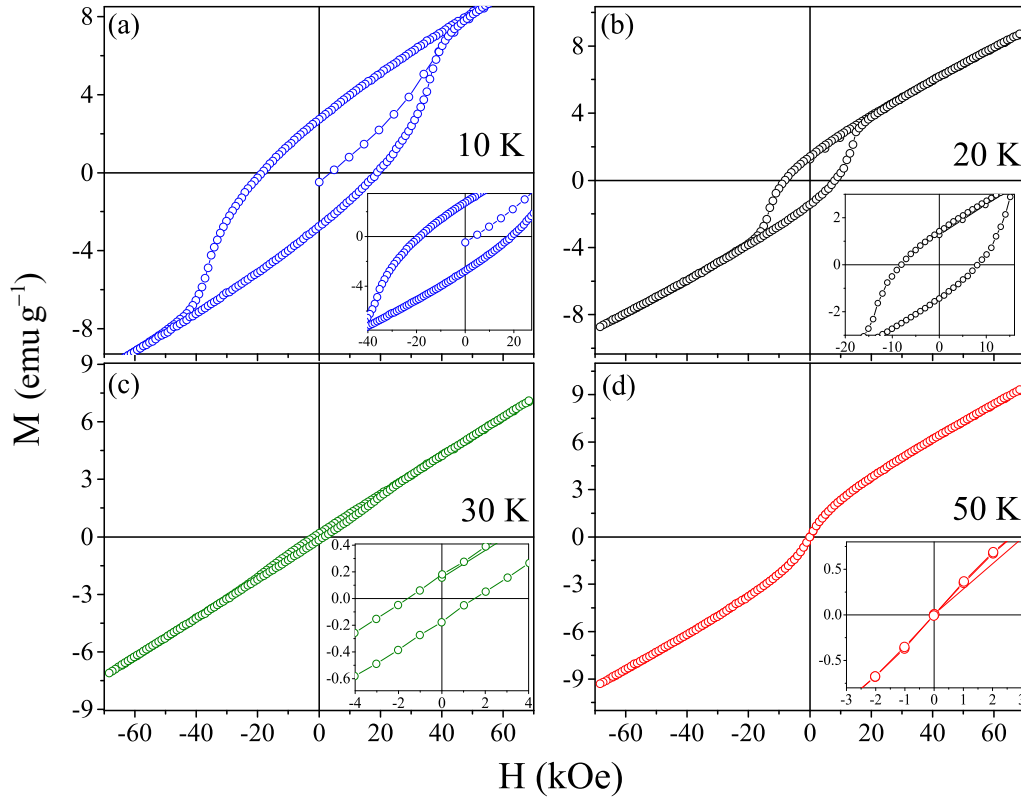FIG. 10. (Color online) The best fit of the relaxation times to the Vogel-Fulcher law in Co_2TiO_4.

FIG. 11. (Color online) Plots of hysteresis loops (M vs H) in Co_2TiO_4 are shown at selected temperatures of (a) 10 K, (b) 20 K, (c) 30 K, and (d) 50 K recorded under ZFC condition. The insets show the zoomed view of M-H loops near origin showing the asymmetry in the loops.

temperatures shown in Fig. 11 show that a weak ferromagnetic component M_{WF} is superimposed on a linear component with M_{WF} strongly temperature dependent. The inset of the Fig. 12 shows asymmetry in the M-H loops measured at 5 K under ZFC and FC (± 20 kOe) protocol. The standard definition of the coercivity is $H_C = (H^+ - H^-)/2$, and loop shift is $H_{EB} = (H^+ + H^-)/2$, where $H^+(H^-)$ are magnetic field values for which $M = 0$, and the remanence M_R for

FIG. 12. (Color online) The hysteresis loops (M vs H) measured at low temperatures 5, 6, 7, 8, and 9 K under ZFC condition. The insets show the asymmetry in the M-H loops measured at 5 K under FC (20 kOe) condition.

the magnetization at $H = 0$ are used along with M_{max}, the measured magnetization at 90 kOe [shown in Figs. 13(a) and 13(b)]. Note that, below 10 K, all the M-H data appear like minor loops; thus, extracted magnitudes of H_C, H_{EB}, and M_R are underestimated significantly. Due to this reason, we do not show the data for $T < 10$ K. Particularly noteworthy are the large magnitudes of $H_C \sim 20$ kOe. In addition, there is a minimum in M_R and M_{max} at 30 K, the temperature for which partial compensation of the two sublattices was indicated in Figs. 5 and 6. Observation of nonzero M_R is evidence for the presence of M_{WF}. We will return to the discussion of these results and their significance later in Sec. V.

For comparison, Fig. 14 shows the temperature dependence of H_C and H_{EB} for the Co_2SnO_4 system. In this case, a hysteresis loop is observed only between 10 and 35 K with a peak in H_C occurring at 20 K, and there is no difference in the magnitude of H_C for the ZFC case and the FC case in which the sample was cooled in $H = 10$ kOe from well above T_N. The exchange bias H_{EB} is observed only for the FC case.

E. Temperature dependence of the specific heat

The plots of the temperature dependence of the specific heat $C_p(T)$ of Co_2TiO_4 measured in $H_{dc} = 0$, 10 and 50 kOe are shown in Fig. 15. From 5 to 28 K, the data were taken at temperature intervals of 2 K and from 28 to 60 K in steps of 1 K. In $H_{dc} = 0$ Oe, a single shoulder in C_p vs T is observed at $T_N = 47.8$ K, very similar to the earlier studies by Ogawa and Waki [20]. In applied field of 10 and 50 kOe, this peak becomes diffuse and shifts by a few degrees to higher temperatures (see
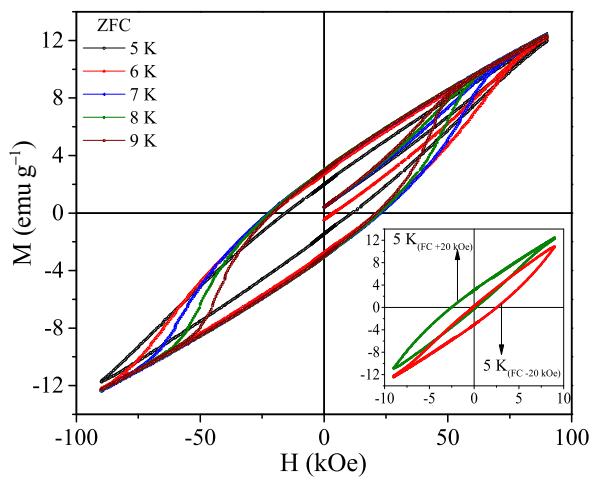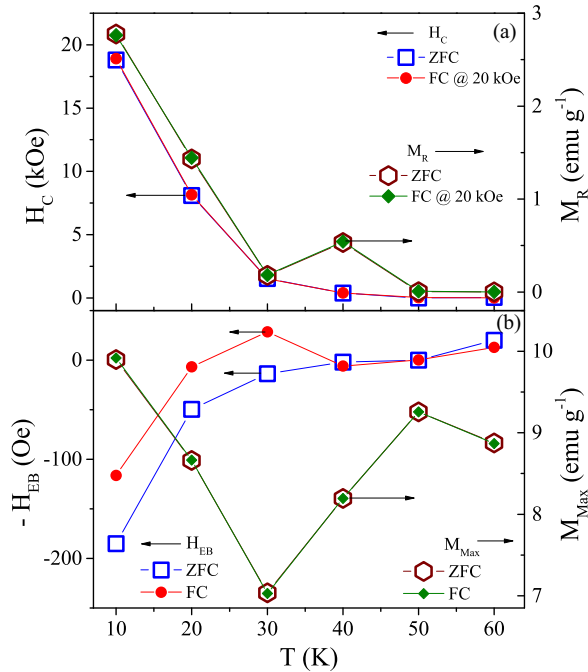
FIG. 13. (Color online) The temperature variation of (a) coercive field $H_C(T)$ and remanence magnetization M_R and (b) exchange bias $H_{EB}(T)$ and high field ($H \sim 90\,\text{kOe}$) magnetization M_{max} measured under both ZFC and FC (20 kOe) conditions in Co_2TiO_4. The lines connecting the data points are visual guides.

FIG. 15. (Color online) The temperature variation of specific heat $C_p(T)$ for the Co_2TiO_4 sample recorded at various magnetic fields ($H_{dc} = 0$, 10, and 50 kOe). The insets show the zoomed view across the ferrimagnetic Néel temperature (T_N) and compensation temperature (T_{comp}).

inset of Fig. 15). Interestingly, another peak is observed at 31.7 K when $H_{dc} = 50\,\text{kOe}$, suggesting some relationship of this peak with the compensation temperature noted above from M vs T data in Figs. 5 and 6.

As discussed in our paper on Co_2SnO_4 [16], magnetic entropy S_M and magnetic specific heat are related by the thermodynamic relation $d(S_M)/dT = C_M/T$. Since it is difficult to accurately separate out the lattice contribution to C_p, we have plotted C_p/T vs temperature in Fig. 16 to get additional information on the magnetic ordering. The slight shift and blurring of T_N at 47.8 K to higher temperatures with increasing H is evident, in addition to a peak near 32 K and a weaker anomaly around 10 K. The fact that the peak in C_p at T_N in $H_{dc} = 0$ is quite weak (almost like a shoulder) compared to peaks observed in typical second-order transitions in three-dimensional (3D) systems is due to unconventional
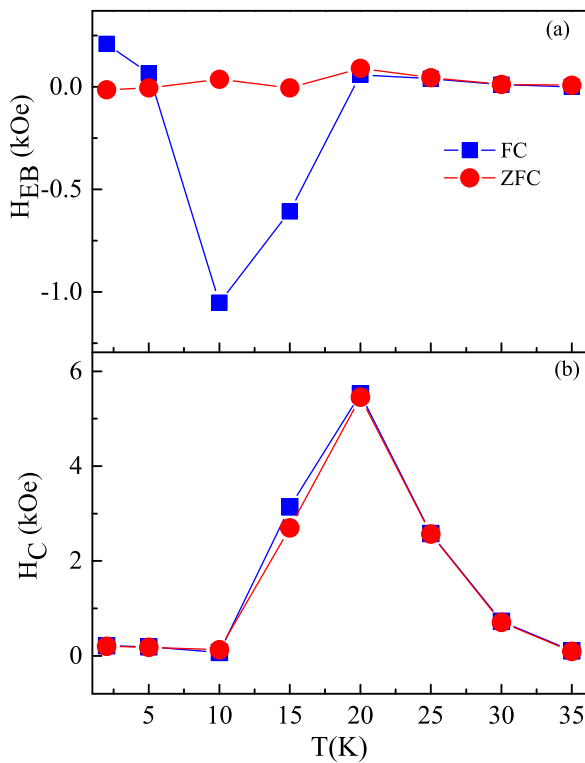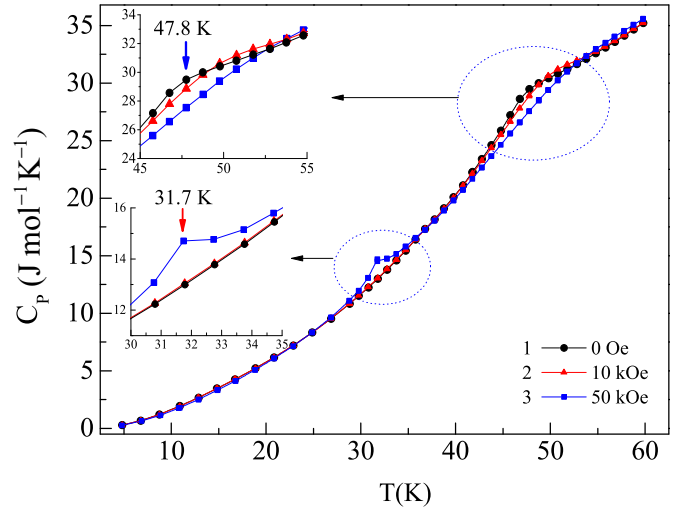

FIG. 14. (Color online) Temperature variations of (a) exchange bias H_{EB} and (b) coercivity H_C in Co_2SnO_4 for the ZFC and FC (@ 10 kOe) cases. The lines connecting the data points are visual guides.
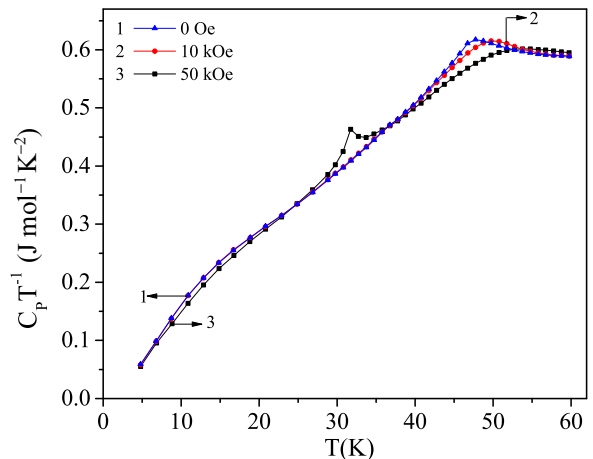

FIG. 16. (Color online) The temperature dependence of C_pT^{-1} for the Co_2TiO_4 sample using the data of Fig. 15.

ordering in Co_2TiO_4 viz. rather in between second-order transition in 3D system and spin-glasses, the latter showing no peak in C_p at T_{SG}. Significance of these results and their comparison with earlier studies of Co_2TiO_4 and our recent studies of Co_2SnO_4 are presented in the following section.

V. DISCUSSION

The paper by Hubsch and Gavoille [17] on the nature of magnetic ordering in Co_2TiO_4 reported $T_N = 55$ K followed by spin-glass ordering at $T_{SG} = 46$ K. However, between 55 and 46 K, the remanence M_R was extremely small, reaching a peak value of only about 0.05 emu/g at 50 K, and then becoming zero again at 46 K. Below 46 K, M_R increased rapidly, peaking at $M_R = 0.7$ emu/g at 40 K before compensation sets in. In the C_p vs T measurements of Ogawa and Waki [20] and in our studies reported here in Fig. 15, a peak in C_p is observed only near 48 K, although under nonzero applied H_{dc}, this feature becomes more diffused and shifts to higher temperatures.

The phenomenon of compensation observed near 32 K in Figs. 5 and 6 confirms the earlier observation of Hubsch and Gavoille [17] However, the compensation in Co_2TiO_4 is not complete in that the magnetization measured at the minimum is not quite zero, and it increases as the magnetic field used for the measurements is increased. In ferrimagnets with different magnetic moments on the A and the B sites and which also have different temperature dependence, a complete compensation or at least a minimum in the observed moment $\mu(T) = \mu(A) - \mu(B)$ could occur at a certain temperature below T_N [15].This is clearly observed here in Co_2TiO_4 in both the measured M (Figs. 5 and 6) and in M_R [Fig. 13(a)]. The estimated magnetic moments on the A and the B sites of Co_2TiO_4 are sufficiently different with $\mu(A) = 3.87\,\mu_B$ and $\mu(B) = 5.19\,\mu_B$, as discussed earlier in Sec. IV A. For comparison, in Co_2SnO_4 with smaller difference in $\mu(A) = 3.87\,\mu_B$ and $\mu(B) = 4.91\,\mu_B$, compensation is not as evident and clear cut, but below about 7 K, there is effectively no remanence or coercivity implying compensation. Another evidence for the difference in the two systems in this regard is the difference in the measured remanence M_R. For Co_2SnO_4, a maximum in $M_R = 0.45$ emu/g is observed near 30 K [16], whereas in Co_2TiO_4, a maximum in $M_R = 3$ emu/g observed near 10 K is a factor of about six larger. The ratio of the observed M_R in Co_2TiO_4 and Co_2SnO_4 scales well with the difference in their $\mu(A)$ and $\mu(B)$ values when normalized with their molecular weights.

The temperature dependence of coercivity $H_C(T)$ and exchange bias $H_{EB}(T)$ shown in Figs. 13(a) and 13(b) is considered next. In the Stoner-Wohlfarth (SW) model of coercivity in single-domain particle, $H_C = K_A/M_S$, where K_A is the magnetocrystalline anisotropy constant and M_S is the saturation magnetization [31]. Below T_N, $K_A \sim (M_S)^n$, where n is system dependent and can be as large as 10 [31]. Therefore, in the SW model, H_C should continue to increase with decrease in temperature below T_N. In the plot of H_C vs T in Fig. 13(a) for Co_2TiO_4, an increase in H_C with a decrease in T is observed, reaching a peak at about 10 K below which H_C decreases, and it is accompanied by the appearance of a very significant

H_{EB}. In real systems, H_C is affected by impurities and grain boundaries which pin down the domain walls and prevent their rotation as the magnetic field is varied. The M vs T plot of Fig. 6 shows that, below T_{comp}, the FC and ZFC curves bifurcate at a certain temperature T_b, which decreases as H_{dc} increases. This is similar to the observation reported in Ni-hydroxide layered systems [32,33], where this phenomenon was associated with the blocking temperature of nanocrystallites. In both Co_2TiO_4 and Co_2SnO_4, the crystallite size is in the micrometer range. However, because of the substitution of the different magnetic ions with different magnetic moments on the B sites, the formation of magnetic clusters is very likely. The bifurcation of the M (FC) and M (ZFC) curves in Figs. 6 and 7 at a specific temperature T_b, which decreases with increase in H_{dc}, may thus be due to freezing of these magnetic clusters. The observations of very large H_C and H_{EB}-like behavior at 10 K in Co_2TiO_4 could thus result from the inability of the spins in the frozen clusters to follow the magnetic field.

Another noteworthy result in Co_2TiO_4 is the lack of saturation of the magnetization in H up to 90 kOe (Figs. 11 and 12). In the results reported by Hubsch and Gavoille [17], lack of saturation was evident even up to 150 kOe. These results suggest noncollinear ordering of spins in Co_2TiO_4. Preliminary neutron diffraction measurements by Hubsch and Gavoille [17] were evidence for the canting of the spins, which is consistent with nonsaturation of the magnetization. Qualitatively, this situation may be akin to that in the spinel Mn_3O_4 for which the two sublattices were found to be inadequate to describe the magnetic structure below T_N [34]. In Co_2TiO_4, the B sites are occupied by two different magnetic ions, Co^{3+} and Ti^{3+}, as reported here; therefore, at least a three-sublattice model is necessary to describe its magnetic structure. Srivastava et al. [7] have discussed a three-sublattice model in which magnitudes of the saturation magnetization and temperature dependence of paramagnetic susceptibility are used to solve for the exchange constants. Since, in Co_2TiO_4, magnetization does not saturate even up to 150 kOe, as noted above, this model cannot be applied to Co_2TiO_4. Thus, determining the nature of magnetic ordering of the spins below T_N in Co_2TiO_4 remains an outstanding challenge, both experimentally and theoretically.

VI. CONCLUDING REMARKS

Results and their analysis on the structural and magnetic properties of Co_2TiO_4 are presented here along with a comparison with the properties of the isostructural compound Co_2SnO_4, reported here as well as in published papers recently [15,16]. The major results are as follows: (i) analysis of the temperature dependence of the dc susceptibilities above T_N using the Néel expression for ferrimagnets yields magnetic moments $\mu(A) = 3.87\,\mu_B$ and $\mu(B) = 5.19\,\mu_B$ (4.91 μ_B) for Co_2TiO_4 (Co_2SnO_4), $\mu(B)$ being significantly different for the two cases; this difference in $\mu(B)$ is the major reason for differences in their magnetic properties; (ii) analysis of the XPS data shows the electronic structure of Co_2TiO_4 to be $[Co^{2+}][Co^{3+}Ti^{3+}]O_4$ as compared to $[Co^{2+}][Co^{2+}Sn^{4+}]O_4$ for Co_2SnO_4. This difference in the electronic structures of

the ions on the B sites is used to explain the difference in the observed $\mu(B)$ values and the lack of definite evidence for the presence of spin-glass transition in Co_2TiO_4 in contrast to the observation in Co_2SnO_4; (iii) a compensation temperature of $T_{comp} \simeq 32$ K is observed for Co_2TiO_4 below which the system retains its ferrimagnetic character. In contrast, a similar compensation point is not observed in Co_2SnO_4, although below 7 K, there is no coercivity or remanence which would be signatures of a compensated state; and (iv) the large magnitudes of the coercivity H_C observed in Co_2TiO_4 in the uncompensated state most likely results from spin clusters. Also, the observed field-dependent magnetization reversal and lack of saturation of the magnetization in Co_2TiO_4 below its T_N in magnetic fields up to 150 kOe suggest complex canting of the spins, which can be best determined by neutron diffraction measurements. It is hoped that the results presented here will provide the motivation for additional investigations.

[1] E. W. Gorter, Phillips Res. Rep. **9**, 295 (1954); F. K. Lotgering, *ibid.* **11**, 190 (1956).

[2] V. G. Harris, A. Geiler, Y. Chen, S. D. Yoon, M. Wu, A. Yang, Z. Chen, P. He, P. V. Parimi, X. Zuo, C. E. Patton, M. Abe, O. Acher, and C. Vittoria, J. Magn. Magn. Mater. **321**, 2035 (2009) and references therein.

[3] D. Fiorani, S. Viticoli, J. L. Dormann, J. L. Tholence, and A. P. Murani, Phys. Rev. B **30**, 2776 (1984).

[4] W. Schiessl, W. Potzel, H. Karzel, M. Steiner, G. M. Kalvius, A. Martin, M. K. Krause, I. Halevy, J. Gal, W. Schäfer, G. Will, M. Hillberg, and R. Wäppling, Phys. Rev. B **53**, 9143 (1996).

[5] C. E. Rodríguez Torres, G. A. Pasquevich, P. Mendoza Zélis, F. Golmar, S. P. Heluani, S. K. Nayak, W. A. Adeagbo, W. Hergert, M. Homann, A. Ernst, P. Esquinazi, and S. J. Stewart, Phys. Rev. B **89**, 104411 (2014).

[6] K. Kamazawa, Y. Tsunoda, H. Kadowaki, and K. Kohn, Phys. Rev. B **68**, 024412 (2003).

[7] C. M. Srivastava, G. Srinivasan, and N. G. Nanadikar, Phys. Rev. B **19**, 499 (1979).

[8] G. Rado and V. Folen, J. Appl. Phys. **31**, 62 (1960).

[9] P. Bercoff and H. Bertorello, J. Magn. Magn. Mater. **169**, 314 (1997).

[10] K. M. Kojima, R. Kadono, M. Miyazaki, M. Hiraishi, I. Yamauchi, A. Koda, Y. Tsuchiya, H. Suzuki, and H. Kitazawa, Phys. Rev. Lett. **112**, 087203 (2014).

[11] G. J. Nilsen, Y. Okamoto, T. Masuda, J. Rodriguez-Carvajal, H. Mutka, T. Hansen, and Z. Hiroi, Phys. Rev. B **91**, 174435 (2015).

[12] M. Reehuis, M. Tovar, D. M. Többens, P. Pattison, A. Hoser, and B. Lake, Phys. Rev. B **91**, 024407 (2015).

[13] M. S. Seehra, V. Singh, S. Thota, B. Prasad, and J. Kumar, Appl. Phys. Lett. **97**, 112507 (2010); M. S. Seehra, V. Singh, and S. Thota, J. Appl. Phys. **110**, 113907 (2011).

[14] P. W. Anderson, Phys. Rev. **102**, 1008 (1956).

[15] S. Thota and M. S. Seehra, J. Appl. Phys. **113**, 203905 (2013); **118**, 129901 (2015).

[16] S. Thota, V. Narang, S. Nayak, S. Sambasivam, B. C. Choi, T. Sarkar, M. S. Andersson, R. Mathieu, and M. S. Seehra, J. Phys.: Condens. Matter **27**, 166001 (2015).

[17] J. Hubsch and G. Gavoille, Phys. Rev. B **26**, 3815 (1982).

[18] G. Gavoille, J. Hubsch, and S. Koutani, J. Magn. Magn. Mater. **102**, 283 (1991).

[19] J. K. Srivastava, J. A. Kulkarni, S. Ramakrishnan, S. Sing, V. R. Marathe, G. Chandra, V. S. Darshane, and R. Vijayaraghavan, J. Phys. C: Solid State **20**, 2139 (1987).

[20] S. Ogawa and S. Waki, J. Phys. Soc. Jpn. **20**, 540 (1965).

[21] J. K. Kwak, K. H. Park, D. Y. Yun, D. U. Lee, T. W. Kim, D. I. Son, J. H. Han, and J. Y. Lee, J. Korean Phys. Soc. **57**, 1803 (2010).

[22] J. G. Kim, D. L. Pugmire, D. Bhattagila, and M. A. Langell, Appl. Surf. Sci. **165**, 70 (2000).

[23] S. C. Petitto, E. M. Marsh, G. A. Carson, and M. A. Langell, J. Mol. Catal. A: Chem. **281**, 49 (2008).

[24] T. J. Chuang, C. R. Brundle, and D. W. Rice, Surf. Sci. **59**, 413 (1976).

[25] Y. Fu, H. Du, S. Zhang, and W. Huang, Mater. Sci. Eng. A **403**, 25 (2005).

[26] E. McCafferty and J. P. Wightman, Surf. Interface Anal. **26**, 549 (1998).

[27] J.-M. Themlin, M. Chtaïb, L. Henrard, P. Lambin, J. Darville, and J. M. Gilles, Phys. Rev. B **46**, 2460 (1992).

[28] J. Xu, P. Gao, and S. T. Zhao, Energy Environ. Sci. **5**, 5333 (2012).

[29] P. N. Shelke, Y. B. Khollam, K. R. Patil, S. D. Gunjal, S. R. Jadkar, M. G. Takwale, and K. C. Mohite, J. Nano. Electron. Phys. **3**, 486 (2011).

[30] S. Ivanov, R. Tellgren, F. Porcher, G. Andre, T. Ericsson, P. Nordblad, N. Sadovskaya, G. Kaleva, E. Politova, M. Baldini, C. Sun, D. Arvanitis, P. Anil Kumar, and R. Mathieu, Mater. Chem. Phys. **158**, 127 (2015).

[31] A. H. Morrish, *The Physical Principles of Magnetism* (Wiley-VCH, New York, 2001), p. 696.

[32] J. D. Rall, M. S. Seehra, and E. S. Choi, Phys. Rev. B **82**, 184403 (2010); J. D. Rall and M. S. Seehra, J. Phys.: Condens. Matter **24**, 076002 (2012).

[33] M. S. Seehra and V. Singh, J. Phys.: Condens. Matter **25**, 356001 (2013).

[34] G. Srinivasan and M. S. Seehra, Phys. Rev. B **28**, 1 (1983).